Chemical Science

ROYAL SOCIETY OF CHEMISTRY

EDGE ARTICLE

View Article Online
View Journal | View Issue

Cite this: *Chem. Sci.*, 2024, **15**, 2655

All publication charges for this article have been paid for by the Royal Society of Chemistry

Received 21st October 2023
Accepted 3rd January 2024

DOI: 10.1039/d3sc05617a

rsc.li/chemical-science

All-catecholate-stabilized black titanium-oxo clusters for efficient photothermal conversion†

Jinle Hou,‡*[a] Nahui Huang,‡[a] Dinesh Acharya,[b] Yuxin Liu,[a] Jiaying Zhu,[a] Jiaxin Teng,[a] Zhi Wang,[b] Konggang Qu,[a] Xianxi Zhang*[a] and Di Sun*[b]

The controlled synthesis of titanium-oxo clusters (TOCs) completely stabilized by organic dye ligands with high stability and superior light absorption remains a significant challenge. In this study, we report the syntheses of three atomically precise catechol (Cat)-functionalized TOCs, $[Ti_2(Cat)_2(OEgO)_2(OEgOH)_2]$ (**Ti2**), $[Ti_8O_5(Cat)_9(^iPrO)_4(^iPrOH)_2]$ (**Ti8**), and $[Ti_{16}O_8(OH)_8(Cat)_{20}]\cdot H_2O\cdot PhMe$ (**Ti16**), using a solvent-induced strategy (HOEgOH = ethylene glycol; ^{i}PrOH = isopropanol; PhMe = toluene). Interestingly, the TiO core of **Ti16** is almost entirely enveloped by catechol ligands, making it the first all-catechol-protected high-nuclearity TOC. In contrast, **Ti2** and **Ti8** have four weakly coordinated ethylene glycol ligands and six weakly coordinated ^{i}PrOH ligands, respectively, in addition to the catechol ligands. **Ti16** is visually evident in its distinctively black appearance, which belongs to black TOCs (B-TOCs) and exhibits an ultralow optical band gap. Furthermore, **Ti16** displays exceptional stability in various media/environments, including exposure to air, solvents, and both acidic and alkaline aqueous solutions due to its comprehensive protection by catechol ligands and rich intra-cluster supramolecular interactions. **Ti16** has superior photoelectric response qualities and photothermal conversion capabilities compared to **Ti2** and **Ti8** due to its ultralow optical band gap and remarkable stability. This discovery not only represents a huge step forward in the creation of all-catecholate-protected B-TOCs with ultralow optical band gaps and outstanding stability, but it also gives key valuable mechanistic insights into their photothermal/electric applications.

Introduction

Titanium-oxo clusters (TOCs) have garnered significant recent attention owing to their fascinating structures and potential applications in water splitting,[1–3] solar cells,[4–7] pollutant degradation,[8,9] and catalysis.[10–15] The investigation of TOCs is also motivated by their relevance to the structural and reactivity models of TiO_2 materials. TOCs are often grown as single crystals for precise structure determination, which is essential for establishing structure–property relationships at the molecular level.[16–18] While numerous TOCs with varying nuclearities and structures[19–26] have been discovered, including high-nuclearity Ti_{42} [27] and Ti_{52},[28] many suffer from sensitivity to moisture due to the presence of alkoxy groups (–OR) derived from solvents or $Ti(OR)_4$ around their TiO cores. These alkoxy groups typically exhibit monodentate or bridging modes and offer insufficient protection. Research efforts to enhance TOC stability have been focused on introducing surface organic ligands, such as carboxylate, calixarene, and phosphonate ligands.[29–32] However, some TOCs still exhibit insufficient stability due to the incomplete shielding of the TiO core. Therefore, there is a pressing need to develop TOCs with comprehensive protection of the TiO core by ligands to improve their stability. Nevertheless, only a few cases have been reported due to challenges in the synthesis process.[33] Zhang *et al.* reported two Ti_{44} clusters,[34] which have outstanding hydrolytic stability compared to other TOCs due to the thorough shielding of the TiO cores by carboxylates.

In addition to hydrolytic stability, another limitation of TOCs is their restricted light absorption, mainly in the ultraviolet region, hindering efficient solar energy utilization.[35,36] Many strategies have been developed to reduce the optical band gaps of TOCs, including metal doping and ligand modification.[37–40] Despite these efforts to create a broad spectrum of colorful TOCs,[41,42] however, achieving TOCs with an optical band gap low enough to allow absorption of the entire visible spectrum remains a significant challenge. It is well known that catechol-

[a]*Shandong Provincial Key Laboratory of Chemical Energy Storage and Novel Cell Technology, School of Chemistry and Chemical Engineering, Liaocheng University, Liaocheng, 252000, People's Republic of China. E-mail: houjinle@lcu.edu.cn; zhangxianxi@lcu.edu.cn*

[b]*School of Chemistry and Chemical Engineering, Shandong University, Jinan, 250100, People's Republic of China. E-mail: dsun@sdu.edu.cn*

† Electronic supplementary information (ESI) available. CCDC 2294728 (**Ti2**), 2294731 (**Ti8**), 2294729 (**Ti16**), and 2294730 (**Ti16-Me**). For ESI and crystallographic data in CIF or other electronic format see DOI: https://doi.org/10.1039/d3sc05617a

‡ These authors contributed equally to this work.

modified TOCs, which serve as models for dye-sensitized TiO_2 in dye-sensitized solar cells (DSSCs), have narrow band gaps due to ligand-to-metal charge transfer (LMCT) from catechol to the TiO core.[43–46] Therefore, catechol is a promising candidate for extending the light absorption of TOCs to the visible light region. Recently, Zhang *et al.* reported a series of unusual black TOCs (B-TOCs) functionalized by 12 and 14 catechol ligands, $\{Ti_{14}Cat_{12}\}$ and $\{Ti_{14}Cat_{14}\}$, respectively, co-protected by carboxylate ligands, which exhibit ultralow optical band gaps and are ultrastable.[47] Although co-protection with mixed ligands enhances the stability and light absorption of TOCs, it increases structural complexity, making active site identification challenging during applications. Therefore, the development of all-catechol-ligand-protected TOCs has become increasingly attractive, particularly for mechanistic research and rational structural design.

Herein, we design and synthesize three TOCs, $[Ti_2(Cat)_2(OEgO)_2(OEgOH)_2]$ (**Ti2**; Cat = catechol and HOEgOH = ethylene glycol), $[Ti_8(\mu_4\text{-}O)_2(\mu_3\text{-}O)_2(\mu_2\text{-}O)(Cat)_9(^{i}PrO)_4(^{i}PrOH)_2]$ (**Ti8**; ^{i}PrOH = isopropanol), and $[Ti_{16}(\mu_3\text{-}O)_4(\mu_3\text{-}OH)_8(\mu_2\text{-}O)_4(Cat)_{20}]\cdot H_2O\cdot PhMe$ (**Ti16**; PhMe = toluene), by adjusting solvent type. Notably, the periphery of **Ti16** is completely encompassed by catechol ligands, resulting in all-catechol-protected high-nuclearity TOCs, a previously unobserved phenomenon in the field of TOCs. In addition, when the functionalized ligand Cat was changed to 3-methylcatechol (MeCat) in the synthetic system of **Ti16**, a **Ti16** analog, $[Ti_{16}(\mu_3\text{-}O)_4(\mu_3\text{-}OH)_8(\mu_2\text{-}O)_4(MeCat)_{20}]$ (**Ti16-Me**), was isolated, confirming the versatility of this method. Additionally, **Ti16** exhibits a lower band gap and excellent stability compared to **Ti2** and **Ti8** because **Ti16** is surrounded and stabilized by 20 catechol ligands, which endow it with superior photoelectric/thermal properties.

Results and discussion

Syntheses and characterization of Ti2, Ti8, and Ti16

Ti2, **Ti8**, and **Ti16** were successfully synthesized in different solvent systems (Scheme 1). **Ti2** was formed by reacting $Ti(^{i}PrO)_4$ and catechol in ethylene glycol at 100 °C for 72 hours, yielding yellow crystals. Upon the solvent being changed to isopropanol, black crystals of octa-nuclear **Ti8** were isolated. Additionally, no crystals formed when toluene was used as the solvent; a substantial amount of amorphous powder was generated. However, the introduction of a small amount of formic acid into toluene led to the isolation of **Ti16** as black crystals (Fig. S1†). Notably, although formic acid does not participate directly in the coordination, its competitive coordination with metals and pH regulation are crucial for the formation of **Ti16**. Additionally, we replaced formic acid with acetic acid, propionic acid, and butyric acid in the synthesis, while keeping all other synthesis parameters unchanged. However, no crystal was obtained, indicating the indispensability of formic acid.

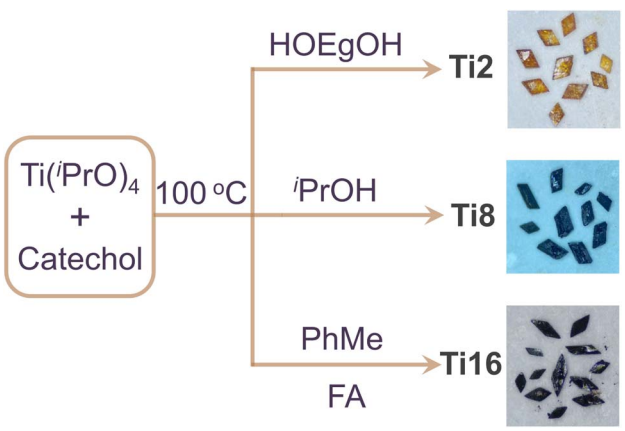

Scheme 1 Schematic diagram of the synthesis for **Ti2**, **Ti8**, and **Ti16** (HOEgOH = ethylene glycol; ^{i}PrOH = isopropanol; PhMe = toluene; FA = formic acid).

The synthesis details and X-ray diffraction data for **Ti2**, **Ti8**, and **Ti16** are shown in the ESI.† The powder X-ray diffraction (PXRD) patterns indicate high crystallinity and phase purity of **Ti2**, **Ti8**, and **Ti16** (Fig. S2–S4†). The infrared (IR) spectra and energy-dispersive X-ray spectroscopy (EDS) analyses for **Ti2**, **Ti8**, and **Ti16** are presented in Fig. S5 and S6.† To investigate the valence states of Ti ions in **Ti2**, **Ti8**, and **Ti16**, X-ray photoelectron spectroscopy (XPS) was carried out, indicating the exclusive presence of Ti^{4+} ions in all of them (Fig. S7–S9†). This observation is consistent with the results obtained from the bond valence sum (BVS) analysis (Table S1†).

Structure analyses of Ti2, Ti8, and Ti16

Single crystal X-ray diffraction (SCXRD) analysis revealed that **Ti2** crystallizes in the monoclinic space group $P2_1/c$ (No. 14), with its asymmetric unit containing half of a cluster. **Ti2** consists of two titanium atoms, two catechol ligands, two double-deprotonated ethylene glycols and two single-deprotonated ethylene glycols (Fig. 1a and b). All Ti atoms in **Ti2** adopt a distorted octahedral coordination geometry (Fig. S10a†). The outer coordination space of **Ti2** is surrounded by two catechol ligands and four ethylene glycols (Fig. 1c). Both catechol ligands adopt the same coordination mode (mode II) (Fig. 1d).

SCXRD reveals that **Ti8** crystallizes in a triclinic system with the space group $P\bar{1}$, and its asymmetric unit contains a complete cluster. **Ti8** consists of eight titanium atoms, two μ_4 bridging O atoms, two μ_3 bridging O atoms, one μ_2 bridging O atom, nine catechol ligands, and six isopropyl molecules (Fig. 1e and f). Two isopropanol molecules are not deprotonated to balance the negative charge of the entire cluster. Significantly, the isopropanol molecules adjacent to the catechol ligands form reasonable hydrogen bonds, ultimately yielding the molecular formula $[Ti_8(\mu_4\text{-}O)_2(\mu_3\text{-}O)_2(\mu_2\text{-}O)(Cat)_9(^{i}PrO)_4(^{i}PrOH)_2]$. Notably, the five titanium atoms (Ti1, Ti2, Ti3, Ti6 and Ti7) are connected by two μ_3-O atoms and one μ_4-O atom to form a $\{Ti_5\}$ trapezoidal layer. This layer is further connected to one Ti8 atom beneath it through a μ_4-O atom, and it is also bonded to two titanium atoms (Ti4 and Ti5) overhead it through one μ_2-O, one μ_3-O, and one μ_4-O, forming an octa-nuclear $\{Ti_8O_5\}$ core. The outer coordination space of $\{Ti_8O_5\}$ is

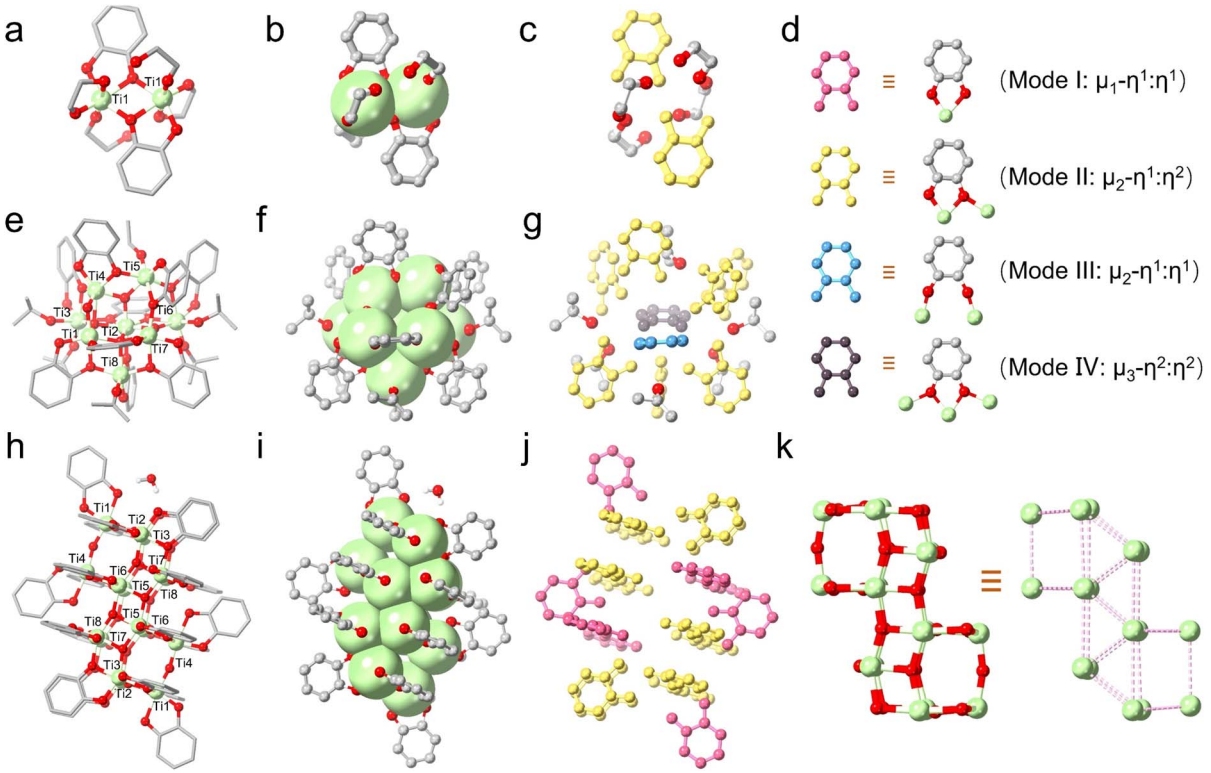

Fig. 1 (a and b) Overall structure of **Ti2**. (c) Distribution of surface ligands on **Ti2**. (d) Binding modes of catecholate ligands. (e and f) Total structure of **Ti8**. (g) Distribution of surface ligands on **Ti8**. (h and i) Total structure of **Ti16**. (j) Distribution of surface ligands on **Ti16**. (k) The $\{Ti_{16}O_{16}\}$ skeletal structure of **Ti16** by removing all ligands. Color code: light green, Ti; red, O; gray, C.

surrounded by nine catechol ligands, four $^{i}PrO^{-}$ anions, and two $^{i}PrOH$ molecules (Fig. 1g). Intriguingly, the nine catechol ligands can be classified into three types based on their coordination modes: seven adopt mode II coordination, one adopts mode III coordination, and one adopts mode IV coordination. All isopropanol molecules adopt terminal coordination modes. Moreover, all titanium atoms within **Ti8** exhibit slightly distorted octahedral geometry, except for the seven-coordinated **Ti2** atom, which shows a pentagonal bipyramid geometry (Fig. S10b†).

SCXRD analysis reveals that **Ti16** crystallizes in a triclinic system with the space group $P\bar{1}$, and its asymmetric unit contains half of a cluster. **Ti16** comprises 16 titanium atoms, 12 μ_3-O/OH, 4 μ_2-O atoms, 20 catechol ligands, and one lattice water molecule (Fig. 1h and i). All Ti atoms in **Ti16** are in an octahedral coordination geometry (Fig. S10c†). Specifically, three titanium atoms (Ti2, Ti6, and Ti7) are joined by one μ_3-O atom to form a $\{Ti_3\}$ triangle. Similarly, another $\{Ti_3\}$ triangle is produced by Ti3, Ti5, and Ti8 atoms linked together by one μ_3-O atom. Two $\{Ti_3\}$ triangles are connected by one μ_2-O atom to generate a $\{Ti_6O_3\}$ triangular prism, which is further connected to Ti5 and Ti8 atoms through two μ_3-O atoms and one μ_2-O atom, forming the $\{Ti_8O_6\}$ cage. Finally, two $\{Ti_8O_6\}$ cages fuse together through four μ_3-O atoms, giving rise to the $\{Ti_{16}O_{16}\}$ core. The $\{Ti_{16}O_{16}\}$ core is entirely encircled by 20 catechol ligands (Fig. 1j and k). Interestingly, 20 catechol ligands exhibit two coordination modes: 8 adopt mode I coordination, while the others adopt mode II coordination. Interestingly, the structure exhibits noteworthy interactions, comprising six pairs of $\pi\cdots\pi$ contacts between the phenyl rings, with centroid–centroid distances calculated to be 3.652, 3.679, and 3.720 Å, respectively. It also features two hydrogen bonding interactions between H_2O and neighboring oxygen atoms of the catechol ligands (Fig. S11†), contributing to the high-stability feature. Notably, all the ligands in **Ti16** are catechols, which contrasts with previously reported Ti_{16}-oxo clusters that contain alkoxide groups from the solvents or the hydrolysis of titanium alkoxides.[48,49] To our knowledge, **Ti16** is the first all-catechol-protected high-nuclearity TOC.

The universality of this method for synthesizing all-catecholate-stabilized TOCs was further demonstrated by replacing the Cat ligand with the MeCat linker. Under identical conditions, black crystals of **Ti16-Me** with high crystallinity were isolated when the Cat ligand was changed to MeCat (Fig. S12†). SCXRD analysis revealed that **Ti16-Me** crystallizes in the triclinic crystal system with the $P\bar{1}$ space group, which is structurally similar to **Ti16**.

Solution behavior of Ti2, Ti8, and Ti16

ESI-MS is a complementary characterization technique to X-ray crystallography, providing valuable insights into the chemical composition and charge state of metal nanoclusters in solution.[50–53] To elucidate the solution behavior of **Ti8**, ESI-MS was performed in positive ion mode. Single crystals of **Ti8**

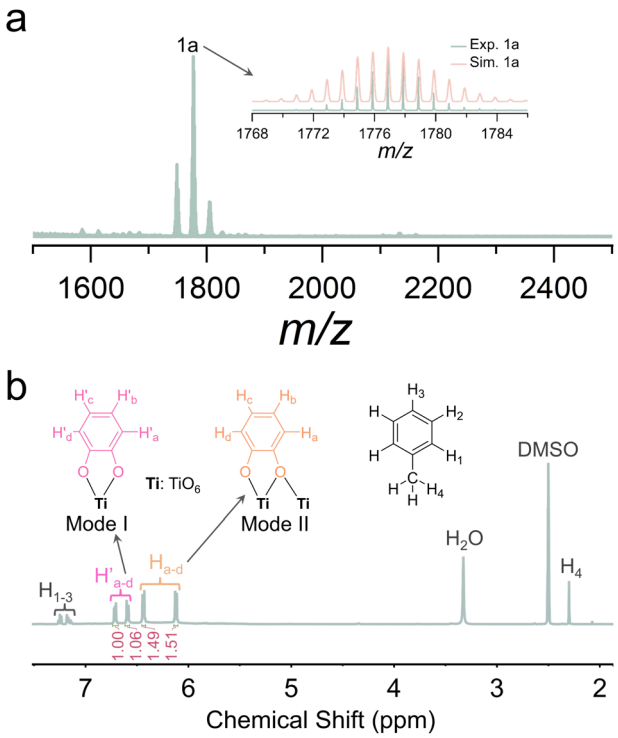

Fig. 2 (a) Positive-ion mode ESI-MS of **Ti8** dissolved in CH_2Cl_2 and insets show the experimental (light green) and simulated (light coral) isotopic distribution patterns for species **1a**. (b) ^{1}H NMR spectrum of **Ti16** in DMSO-d_6.

were dissolved in CH_2Cl_2 and subjected to mass spectrometry analysis. The most prominent peak, **1a**, centered at 1776.8652, is assigned to $[Ti_8O_4(Cat)_8(^iPrO)_5(CH_2Cl_2)_2]^+$ (calcd m/z = 1776.8901), corresponding to the loss of one catechol ligand and one $^iPrO^-$ from **Ti8** (Fig. 2a). Additionally, we studied the solution behavior of **Ti16** using ESI-MS. Unfortunately, we did not achieve the desired results.

As an alternative, NMR is a unique and powerful technique that provides some dynamic behavior in solution.[54,55] Hence, ^{1}H NMR experiments of **Ti2** and **Ti16** were conducted. The ^{1}H NMR spectrum of **Ti2** exhibits peaks at 6.10–6.14 ppm and 6.42–6.46 ppm, corresponding to the H atoms (H_{a-d}) of catechol ligands adopting the mode II coordination mode, given that catechol ligands of **Ti2** exclusively display the mode II coordination mode (Fig. S13†). Additionally, in the ^{1}H NMR spectrum of **Ti16**, H_{a-d} signals are also present, accompanied by two sets of new peaks at 6.57–6.61 ppm and 6.70–6.74 ppm (Fig. 2b). Considering the coexistence of mode I and mode II coordination modes of catechol ligands in **Ti16**, peaks at 6.57–6.61 ppm and 6.70–6.74 ppm can be attributed to the H atoms (H'_{a-d}) of catechol ligands adopting the mode I coordination mode. Furthermore, peak integration reveals a H_{a-d} : H'_{a-d} molar ratio of approximately 3 : 2, which matches the theoretical ratio of catechol ligands in mode II : mode I in **Ti16**, which is 12 : 8. Signals attributed to toluene are observed at 2.30 ppm (H_4) and 7.13–7.27 ppm (H_{1-3}), indicating the presence of toluene solvent in the lattice of **Ti16**. Consequently, the ^{1}H NMR results confirm the solution stability of **Ti16**.

Stability of Ti2, Ti8, and Ti16

The stability of metal nanoclusters is essential for accurately assessing their catalytic performance and exploring their potential for industrial applications.[56] In general, the surfaces of many TOCs, such as the well-known Ti_{34} and Ti_{42}, are enveloped by alkoxide or a combination of alkoxide and carboxylate ligands, resulting in poor stability in air or under hydrolytic conditions.[27,57] Unlike many other PTCs, which are prone to instability, the presented **Ti16**, entirely shielded by 20 catechol ligands and additionally reinforced by rich intracluster supramolecular interactions, offers exceptional stability against air exposure, various solvents, and a wide pH range in acidic or basic aqueous solutions. This exceptional stability makes **Ti16** a promising candidate for heterogeneous catalysis in aqueous/organic solvent media. Specifically, **Ti16** remained in its crystalline structure for at least one month when exposed to air, as evidenced by unchanged PXRD patterns. It also remains unaffected by common solvents such as dichloromethane, chloroform, acetonitrile, isopropanol, and toluene (Fig. 3a). Furthermore, its crystallinity persists in aqueous environments with pH values ranging from 1 to 11, as indicated by the consistent PXRD patterns (Fig. 3b). Moreover, the IR patterns of **Ti16** soaked in aqueous solution/common solvents are consistent with those of the original **Ti16**, further indicating its excellent stability (Fig. S14 and S15†).

Similar notable improvements in pH stability were also observed in **Ti8** (Fig. S16 and S17†). However, **Ti8** was unstable after exposure to the air for one week and in solvent, as confirmed by the changed PXRD pattern (Fig. S18†). This is because the surface of **Ti8** has 6 weakly coordinated ^{i}PrOH ligands, resulting in inadequate protection. Similarly, **Ti2** also became unstable after a week of air exposure due to its surface featuring 4 weakly coordinated ethylene glycol ligands. The presence of a small amount of monodentate solvent ligands in **Ti2** and **Ti8** can easily detach, leaving the Ti sites exposed, which renders them unstable. In addition, thermogravimetric analysis (TGA) was performed to evaluate the thermal stability of **Ti2**, **Ti8**, and **Ti16** (Fig. S19†). The corresponding findings reveal that their structural integrity can be maintained at approximately 198 °C, 246 °C, and 349 °C, respectively. Notably, **Ti16** exhibits excellent resistance to high temperatures. Therefore, the impressive stability of **Ti16** should be attributed to the intensive protective effect of catechol ligands and rich intracluster supramolecular interactions. As shown in Table S2,† previously reported TOCs functionalized with catecholate ligands are typically coordinated with the alkoxide groups from the $Ti(OR)_4$ precursor or the alcohol solvents. These TOCs typically exhibit poor stability and rapidly lose their crystallinity when exposed to air, immersed in water, or even stored in their mother solutions.

Photoelectric response properties

Analyzing the broader literature, it's noted that TOCs decorated with catechol-based ligands display a narrowed band gap compared to those without such functional groups.[43–47] Coppens and Benedict pioneered the preparation of TOCs with

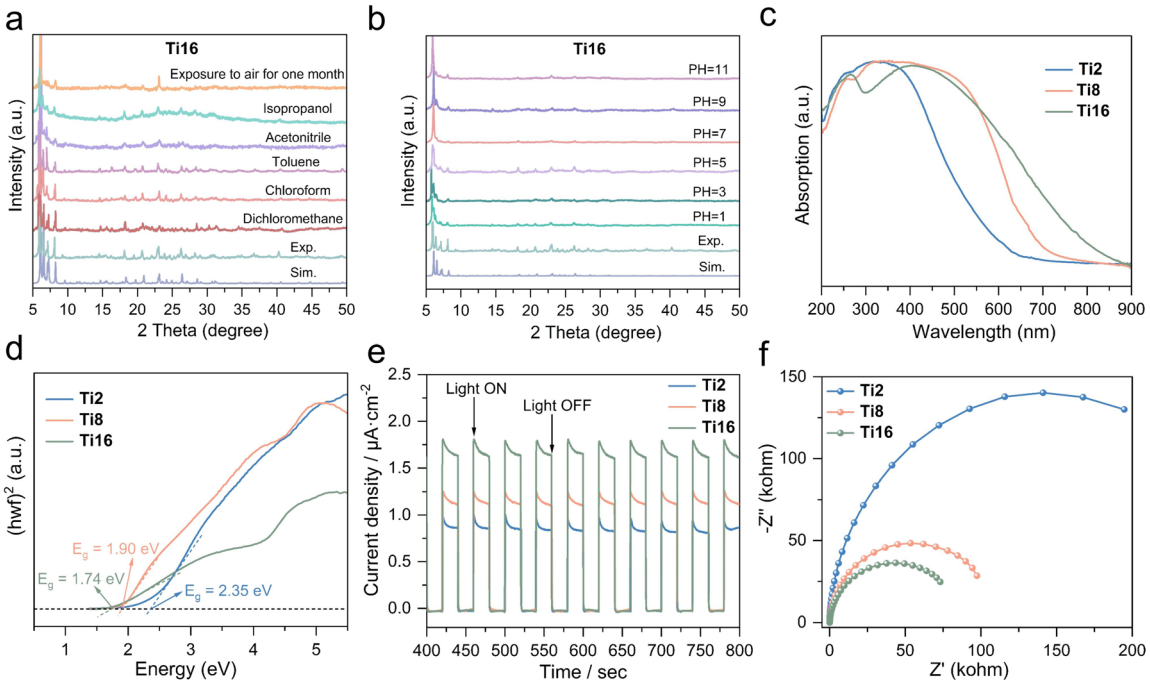

Fig. 3 PXRD pattern of **Ti16** under different conditions. (a) Exposed to air for a month and soaked in common organic solvents for 48 hours. (b) Soaked in water solutions with pH ranging from 1 to 11 for 48 hours. (c) Solid-state UV-visible absorption spectra of **Ti2**, **Ti8**, and **Ti16**. (d) Tauc plots of **Ti2**, **Ti8**, and **Ti16**. (e) Transient photocurrent responses of **Ti2**, **Ti8**, and **Ti16** under Xe lamp irradiation. (f) Electrochemical impedance spectroscopy (EIS) Nyquist plots of **Ti2**, **Ti8**, and **Ti16**.

catechol ligands as photosensitizers, demonstrating that charge transfer occurs from catechol to the Ti(IV) cluster core, leading to the deep-red color and narrowed band gap.[43] Recently, Zhang *et al.* reported a series of unusual B-TOCs with ultralow optical band gaps employing catechol ligands in the presence of carboxylate ligands.[47] Therefore, we envision that introducing more catechols into TOCs may effectively alter their light absorption range to include visible and even infrared light regions.

To assess the light absorption capacity of **Ti2**, **Ti8**, and **Ti16**, the solid-state UV-visible absorption spectrum was employed (Fig. 3c). The spectrum clearly shows that **Ti2** and **Ti8** exhibit broad absorption bands with edge wavelengths of 635 nm and 749 nm, respectively. However, **Ti16** reveals broader absorption bands with edge wavelengths extending to 872 nm. This means that the light absorption of **Ti16** covers the visible light region and extends to the infrared light region. It is widely accepted that the UV-light absorption band is primarily due to the O → Ti charge transfer in the TiO core.[58] It has been shown that including catechol ligands can significantly alter the light absorption of TOCs. Furthermore, two reported cases of 16-nuclei TOCs,[34,48] which are surrounded by alkoxide or a combination of alkoxide and carboxylate ligands (Fig. S20†), exhibit a colorless appearance, whereas **Ti16** appears black. This observation validates the importance of introducing catechol into TOCs for enhanced light absorption performance. Based on the Kubelka–Munk function $(\alpha h\upsilon)^2 = \kappa(h\upsilon - E_g)$ (E_g is the band gap (eV), h is the Planck's constant (J s), υ is the light frequency (s^{-1}), κ is the absorption constant and α is the absorption coefficient),[59] the optical bandgaps were estimated to be 2.35 (**Ti2**), 1.90 (**Ti8**), and 1.74 eV (**Ti16**), indicating their potential to exhibit characteristics akin to semiconductors (Fig. 3d).

The band gaps of the TOCs presented here decrease as the ratio of catechol to Ti increases. For example, the band gap of **Ti2** is 2.35 eV when the catechol : Ti = 1 : 1. Still, it decreases to 1.90 eV for **Ti8** with catechol : Ti = 9 : 8 and further decreases to 1.74 eV for **Ti16** with catechol : Ti = 20 : 16. This indicates the significant effect of the number of catechol groups on the band gap of TOCs.

To assess the efficiency of photo-induced electron transfer and charge separation, we conducted transient short-circuit photocurrent measurements for **Ti2**, **Ti8**, and **Ti16** in a typical three-electrode system (Fig. 3e). The system consisted of TOC-modified indium tin oxide (ITO) glass as the working electrode, Ag/AgCl as the reference electrode, and a platinum wire as the counter electrode. These measurements were performed in a 0.20 mol L^{-1} Na_2SO_4 electrolyte solution under illumination with a 150 W high-pressure xenon lamp, maintaining a bias potential of 0.6 V. The photocurrent responses of **Ti2**, **Ti8**, and **Ti16** were observed, and they were in the order of **Ti16** (1.63 μA cm^{-2}) > **Ti8** (1.11 μA cm^{-2}) > **Ti2** (0.86 μA cm^{-2}). **Ti16** exhibited a higher photocurrent density than **Ti2** and **Ti8**, demonstrating that it can capture more photogenerated electrons and suppress the recombination of photoinduced electrons and holes.[60] The stability of the electrode was further confirmed by comparing the IR spectra. After the photocurrent tests, the IR spectra (Fig. S21–S23†) of the samples were essentially identical to those of

the original samples. This indicates that these samples did not undergo decomposition during the photocurrent measurements. We performed electrochemical impedance spectroscopy (EIS) measurements to further confirm the charge separation efficiency. As depicted in Fig. 3f, the Nyquist plot for **Ti16** is smaller than that for **Ti2** and **Ti8**, suggesting that the interfacial charge transfer process in **Ti16** is more rapid than in **Ti2** and **Ti8**.

To better comprehend the disparate optical properties of these catechol-functionalized TOCs, density functional theory (DFT) calculations were performed on **Ti2**, **Ti8**, and **Ti16**, respectively. As shown in Fig. 4 and S24,† an analysis of the atomic orbital (AO) characteristics in the composition of the frontier orbitals of **Ti2**, **Ti8**, and **Ti16** was provided. The electron density of HOMOs of these TOCs is primarily located on the Ti 3d orbitals of the Ti-oxo cores, while LUMOs are predominantly dominated by contributions from the catechol ligands. The DFT calculation results suggest that the LUMO → HOMO transition of these TOCs mainly involves charge transfer from the catechol groups to the Ti-oxo cores. The electronic structures of **Ti2**, **Ti8**, and **Ti16** were compared to determine the effect of the metal and ligand on the TOCs. The computed HOMO–LUMO gap is as follows: **Ti2** (4.0189 eV) > **Ti8** (3.0540 eV) > **Ti16** (2.9318 eV). The small difference in the HOMO–LUMO gap of **Ti16** implies a narrow band gap resulting from the LUMO–HOMO transition.

It is well known that charge transfer from ligands to a metal in a cluster can lead to a lower band gap. This phenomenon can be explained by molecular orbital theory. In these TOCs, molecular orbitals are formed by combining atomic orbitals from Ti metal and ligands. When charge transfer occurs from ligands to the Ti metal, the energy levels of the ligand orbitals can shift closer to the metal orbitals. This can result in new molecular orbitals with altered energy levels. Specifically, charge transfer from ligands to the metal can populate the lower-energy molecular orbitals, reducing the energy gap between the HOMO and LUMO. A smaller energy gap translates to a lower band gap, making it easier for electrons to transition between these levels and absorb lower-energy photons. In **Ti16**, additional ligands populate the lower-energy molecular orbitals, which reduces the energy gap between orbitals. When we move to the molecular orbital coefficient, **Ti16** has a positive coefficient (0.66170, 0.11074), which indicates the constructive combination of the atomic orbital, enhancing electron density in the molecular orbital, whereas **Ti2** and **Ti8** have a positive as well as a negative coefficient. Here, the negative coefficient represents a destructive combination which reduces electron density in that part of the molecular orbital. Due to this constructive combination of atomic orbitals the HOMO–LUMO gap is decreased which ultimately gives a narrow optical band gap of **Ti16**.

To verify this, we also compared the frontier molecular orbital (FMO) properties of the ground (S_0) and excited state (S_1) for **Ti2**, **Ti8**, and **Ti16** using time-dependent density functional theory (TD-DFT). Excitingly, **Ti16** (2.44 eV) also has a lower energy gap between the ground state (S_0) and excited states (S_1) than **Ti2** (3.24 eV) and **Ti8** (2.49 eV). The computational results show that including catechol ligands can significantly alter the energy gaps and optical properties of TOCs.

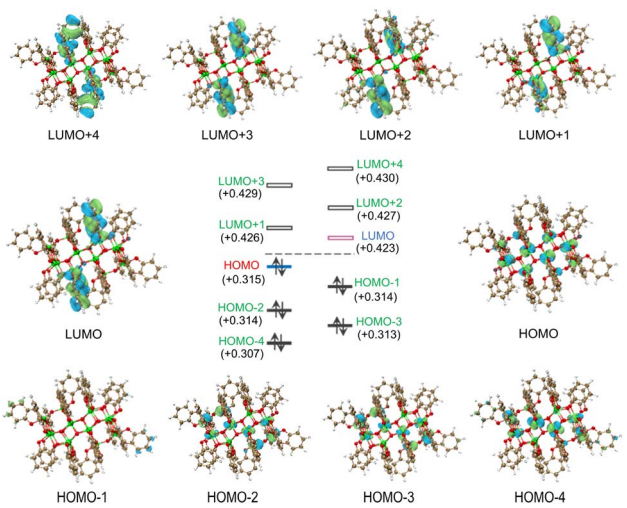

Fig. 4 Iso-surface plots (iso-density value = 0.02 a.u.) of molecular orbitals of Ti16 and their corresponding energy levels.

Photothermal conversion studies

Photothermal energy conversion is a key approach to harnessing light energy. In this process, materials absorb light energy and convert it into heat energy for various applications, including water evaporation, photothermal catalysis, and biomedicine.[61,62] Therefore, designing effective light-absorbing materials is essential for the application of photothermal energy conversion. Encouraged by the efficient visible absorption and excellent stability of these TOCs, we further investigated their photothermal conversion properties. Generally, energy transitions in photophysical processes are primarily depicted by the Jablonski diagram, which includes the following procedures: excitation (or absorption), vibrational relaxation (heat release), radiative emission (fluorescence), and non-radiative transition (heat release).[63–65] No fluorescence was observed for **Ti2**, **Ti8**, and **Ti16**. Therefore, absorption must be considered as the primary factor influencing photothermal conversion performance.

The photothermal conversion performance of the three TOCs was examined in both crystalline and solution states. This is the first time that the photothermal potential of TOCs has been demonstrated. Initially, the photothermal performance of **Ti2**, **Ti8**, and **Ti16** was assessed by dissolving their crystals in *N*,*N*-dimethylformamide (DMF) (c = 0.60 mM) individually and monitoring the temperature changes of the solutions under laser irradiation at 450 nm (0.6 W cm^{-2}). The temperature responses of the solutions and the corresponding thermal images of the three TOCs were better visualized using real-time thermal imaging. As illustrated in Fig. 5a, the temperature of **Ti16** rapidly increased to 67.9 °C after 5 minutes of irradiation. In contrast, the temperatures of both **Ti2** and **Ti8** solutions reached the maximum values of 54.4 °C and 60.9 °C under the same conditions. This result indicates that **Ti16** exhibits

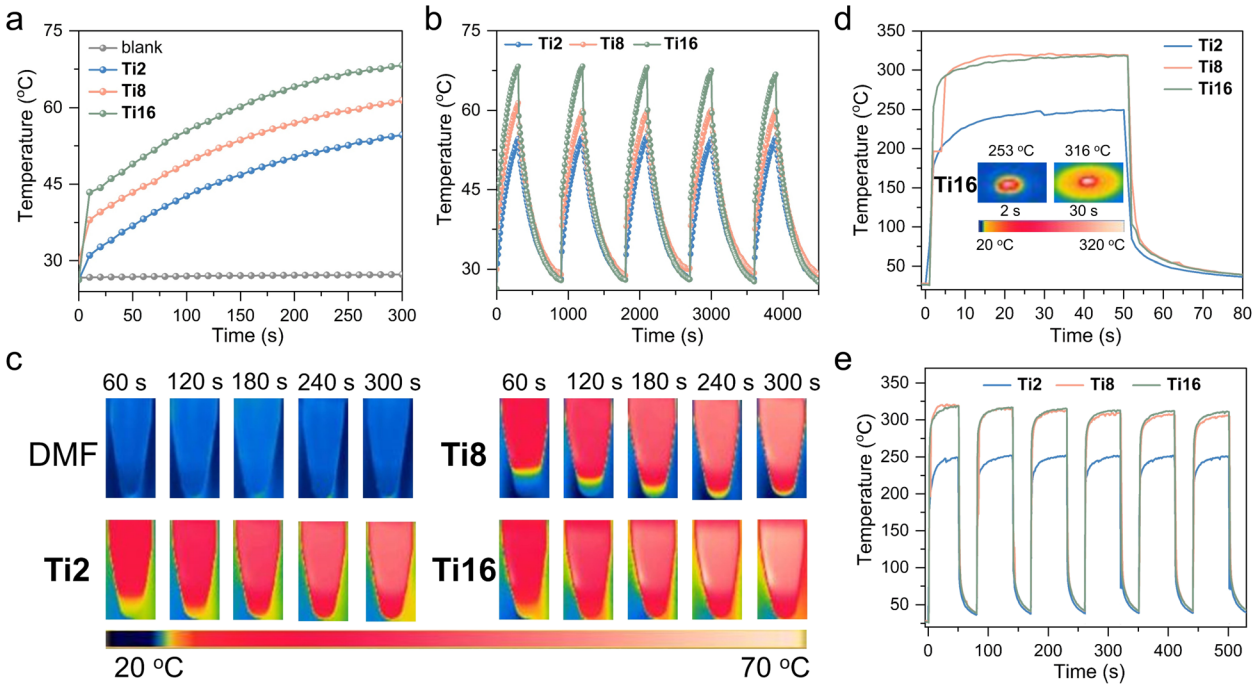

Fig. 5 (a) Photothermal conversion of DMF solution of **Ti2**, **Ti8**, and **Ti16**. (b) Photothermal cycling measurement of DMF solution of **Ti2**, **Ti8**, and **Ti16**. (c) IR thermal images of DMF and DMF solutions of **Ti2**, **Ti8**, and **Ti16**. All measurements were conducted at a concentration of 0.60 mM upon 450 nm laser irradiation (0.6 W cm^{-2}) for (a)–(c). (d) Photothermal conversion of **Ti2**, **Ti8**, and **Ti16** crystals. Insets: thermal images of **Ti16** at various irradiation times. (e) Photothermal cycling measurement of **Ti2**, **Ti8**, and **Ti16** crystals. All measurements were conducted with 450 nm laser irradiation (0.6 W cm^{-2}) at a distance of 15 cm for (d) and (e).

superior photothermal conversion. The photothermal conversion stability of **Ti2**, **Ti8**, and **Ti16** was assessed through five heating and cooling cycles, which showed no significant temperature decay (Fig. 5b). As depicted in Fig. 5c, the thermal images display the photothermal effect of **Ti2**, **Ti8**, and **Ti16** solutions dissolved in DMF.

Moreover, the photothermal properties of **Ti2**, **Ti8**, and **Ti16** crystals were assessed by exposing their crystalline samples to irradiation with a 450 nm laser (0.6 W cm^{-2}) at a distance of 15 cm. Noteworthily, the temperature of **Ti16** crystals reached 253 °C in 2 s. The heating rate (126.5 °C s^{-1}) was higher than that of **Ti8** (98 °C s^{-1}) and **Ti2** (89 °C s^{-1}). It is comparable to the heating rates of most reported photothermal materials (Table S3†). The temperature of **Ti2**, **Ti8**, and **Ti16** reached the maximum values of 249 °C, 319 °C, and 317 °C, respectively, under the same conditions, demonstrating their excellent photothermal conversion properties (Fig. 5d). While **Ti8** and **Ti16** achieved similar maximum temperatures, the heating rate of **Ti16** surpassed that of **Ti8**. Both also show outstanding photothermal stability, as seen by the barely changed maximum temperature after six heating and cooling cycles (Fig. 5e).

Conclusions

In summary, utilizing a solvent-induced approach, we have successfully synthesized three atomically precise catechol-functionalized TOCs, **Ti2**, **Ti8**, and **Ti16**. Notably, **Ti16** stands out as the first TOC entirely enveloped by catechol ligands, resulting in its distinctive black appearance, which suggests an exceptionally low optical band gap. Moreover, **Ti16** exhibits outstanding stability in various environments, including exposure to air, solvents, and both acidic and alkaline aqueous solutions, thanks to its comprehensive protection by catechol ligands and rich intra-cluster supramolecular interactions. Furthermore, **Ti16** demonstrates superior photoelectric response properties and photothermal conversion capabilities compared to **Ti2** and **Ti8**. This enhanced performance is primarily attributed to its narrow band gap and high stability. This research not only offers a practical approach for producing high-nuclearity B-TOCs with ultralow band gaps and strength for exceptional photoelectric/thermal applications, but it also sheds light on the structure–property correlations of black titanium oxide materials.

Data availability

Main experimental data are provided within the main text and the ESI.†

Author contributions

J. L. Hou, X. X. Zhang, and D. Sun proposed the research project and guided the experiments. N. H. Huang, J. L. Hou, J. X. Teng, and K. G. Qu conducted the synthesis and characterization of complexes and contributed to the drafting of the manuscript. Y. X. Liu and J. Y. Zhu performed the photoelectric and

photothermal experiments and related characterization studies. D. Acharya performed computational work and analysis. Z. Wang and D. Sun provided supervision, reviewed, and edited the manuscript. All authors have reviewed and made contributions to this paper.

Conflicts of interest

There are no conflicts to declare.

Acknowledgements

This work was financially supported by the National Natural Science Foundation of China (Grant No. 22325105, 22201159, 22171164, 91961105, 92361301, and 52261135637) and the Natural Science Foundation of Shandong Province (No. ZR2021QB077).

Notes and references

1 Z. Jiang, J. Liu, M. Gao, X. Fan, L. Zhang and J. Zhang, Assembling Polyoxo-Titanium Clusters and CdS Nanoparticles to a Porous Matrix for Efficient and Tunable H_2-Evolution Activities with Visible Light, *Adv. Mater.*, 2017, **29**, 1603369.

2 X. Fan, J. Wang, K. Wu, L. Zhang and J. Zhang, Isomerism in Titanium-Oxo Clusters: Molecular Anatase Model with Atomic Structure and Improved Photocatalytic Activity, *Angew. Chem., Int. Ed.*, 2019, **58**, 1320–1323.

3 C. Wang, C. Liu, L.-J. Li and Z.-M. Sun, Synthesis, Crystal Structures, and Photochemical Properties of a Family of Heterometallic Titanium Oxo Clusters, *Inorg. Chem.*, 2019, **58**, 6312–6319.

4 C. Zhao, Z. Zhang, F. Han, D. Xia, C. Xiao, J. Fang, Y. Zhang, B. Wu, S. You, Y. Wu and W. Li, An Organic–Inorganic Hybrid Electrolyte as a Cathode Interlayer for Efficient Organic Solar Cells, *Angew. Chem., Int. Ed.*, 2021, **133**, 8607–8612.

5 G.-B. Xiao, X. Mu, S. Zhou, L. Zhu, Y. Peng, Q. Liang, X. Zou, J. Zhang, L. Zhang and J. Cao, Directional Transformation of Heterometallic Oxo Clusters: A New Approach to Prepare Wide-Bandgap Cathode Interlayers for Perovskite Solar Cells, *Angew. Chem., Int. Ed.*, 2023, **62**, e202218478.

6 F. Pei, S. Dai, B. Guo, H. Xie, C. Zhao, J. Cui, X. Fang, C. Chen, N. Zheng and F. Pei, Titanium–oxo cluster reinforced gel polymer electrolyte enabling lithium–sulfur batteries with high gravimetric energy densities, *Energy Environ. Sci.*, 2021, **14**, 975–985.

7 G. Zhang, Q. Chen, C. Xie, Y. Wang, C. Zhao, C. Xiao, Y. Wei and W. Li, Mechanical-robust and recyclable polyimide substrates coordinated with cyclic Ti-oxo cluster for flexible organic solar cells, *npj Flexible Electron.*, 2022, **6**, 37.

8 J.-J. Liu, S.-N. Sun, J. Liu, Y. Kuang, J.-W. Shi, L.-Z. Dong, N. Li, J.-N. Lu, J.-M. Lin, S.-L. Li and Y.-Q. Lan, Achieving High-Efficient Photoelectrocatalytic Degradation of 4-Chlorophenol *via* Functional Reformation of Titanium-Oxo Clusters, *J. Am. Chem. Soc.*, 2023, **145**, 6112–6122.

9 L. Zhou, S. Dai, S. Xu, Y. She, Y. Li, S. Leveneur and Y. Qin, Piezoelectric effect synergistically enhances the performance of Ti_{32}-oxo-cluster/$BaTiO_3$/CuS p-n heterojunction photocatalytic degradation of pollutants, *Appl. Catal., B*, 2021, **291**, 120019.

10 N. Li, J.-J. Liu, J.-W. Sun, B.-X. Dong, L.-Z. Dong, S.-J. Yao, Z. Xin, S.-L. Li, Y.-Q. Lan and N. Li, Calix[8]arene-constructed stable polyoxo-titanium clusters for efficient CO_2 photoreduction, *Green Chem.*, 2020, **22**, 5325–5332.

11 J.-J. Liu, N. Li, J.-W. Sun, J. Liu, L.-Z. Dong, S.-J. Yao, L. Zhang, Z.-F. Xin, J.-W. Shi, J.-X. Wang, S.-L. Li and Y.-Q. Lan, Ferrocene-Functionalized Polyoxo-Titanium Cluster for CO_2 Photoreduction, *ACS Catal.*, 2021, **11**, 4510–4519.

12 N. Li, J.-M. Lin, R.-H. Li, J.-W. Shi, L.-Z. Dong, J. Liu, J. He and Y.-Q. Lan, Calix[4]arene-Functionalized Titanium-Oxo Compounds for Perceiving Differences in Catalytic Reactivity Between Mono- and Multimetallic Sites, *J. Am. Chem. Soc.*, 2023, **145**, 16098–16108.

13 M.-Y. Gao, H. Bai, X. Cui, S. Liu, S. Ling, T. Kong, B. Bai, C. Hu, Y. Dai, Y. Zhao, L. Zhang, J. Zhang and Y. Xiong, Precisely Tailoring Heterometallic Polyoxotitanium Clusters for the Efficient and Selective Photocatalytic Oxidation of Hydrocarbons, *Angew. Chem., Int. Ed.*, 2022, **134**, e202215540.

14 C. Liu, H. Niu, D. Wang, C. Gao, A. Said, Y. Liu, G. Wang, C.-H. Tung and Y. Wang, S-Scheme Bi-oxide/Ti-oxide Molecular Hybrid for Photocatalytic Cycloaddition of Carbon Dioxide to Epoxides, *ACS Catal.*, 2022, **12**, 8202–8213.

15 S. E. Brown, I. Mantaloufa, R. T. Andrews, T. J. Barnes, M. R. Lees, F. De Proft, A. V. Cunha, S. D. Pike and S. E. Brown, Photoactivation of titanium-oxo cluster $[Ti_6O_6(OR)_6(O_2C^tBu)_6]$: mechanism, photoactivated structures, and onward reactivity with O_2 to a peroxide complex, *Chem. Sci.*, 2023, **14**, 675–683.

16 P. Coppens, Y. Chen and E. Trzop, Crystallography and Properties of Polyoxotitanate Nanoclusters, *Chem. Rev.*, 2014, **114**, 9645–9661.

17 N. Li, P. D. Matthews, H.-K. Luo, D. S. Wright and N. Li, Novel properties and potential applications of functional ligand-modified polyoxotitanate cages, *Chem. Commun.*, 2016, **52**, 11180–11190.

18 L. Rozes, C. Sanchez and L. Rozes, Titanium oxo-clusters: precursors for a Lego-like construction of nanostructured hybrid materials, *Chem. Soc. Rev.*, 2011, **40**, 1006–1030.

19 U. Schubert, Titanium-Oxo Clusters with Bi- and Tridentate Organic Ligands: Gradual Evolution of the Structures from Small to Big, *Chem.–Eur. J.*, 2021, **27**, 11239–11256.

20 G. Zhang, C. Liu, D.-L. Long, L. Cronin, C.-H. Tung and Y. Wang, Water-Soluble Pentagonal-Prismatic Titanium-Oxo Clusters, *J. Am. Chem. Soc.*, 2016, **138**, 11097–11100.

21 G. Zhang, W. Li, C. Liu, J. Jia, C.-H. Tung and Y. Wang, Titanium-Oxide Host Clusters with Exchangeable Guests, *J. Am. Chem. Soc.*, 2017, **140**, 66–69.

22 M.-H. Du, S.-H. Xu, G.-J. Li, H. Xu, Y. Lin, W.-D. Liu, L.-S. Long, L.-S. Zheng and X.-J. Kong, Modification of

Multi-Component Building Blocks for Assembling Giant Chiral Lanthanide-Titanium Molecular Rings, *Angew. Chem., Int. Ed.*, 2022, **134**, e202116296.

23 C. Zhao, Y.-Z. Han, S. Dai, X. Chen, J. Yan, W. Zhang, H. Su, S. Lin, Z. Tang, B. K. Teo and N. Zheng, Microporous Cyclic Titanium-Oxo Clusters with Labile Surface Ligands, *Angew. Chem., Int. Ed.*, 2017, **56**, 16252–16256.

24 N. Li, J. Liu, J.-J. Liu, L.-Z. Dong, S.-L. Li, B.-X. Dong, Y.-H. Kan and Y.-Q. Lan, Self-Assembly of a Phosphate-Centered Polyoxo-Titanium Cluster: Discovery of the Heteroatom Keggin Family, *Angew. Chem., Int. Ed.*, 2019, **58**, 17260–17264.

25 Y.-P. He, L.-B. Yuan, G.-H. Chen, Q.-P. Lin, F. Wang, L. Zhang and J. Zhang, Water-Soluble and Ultrastable Ti_4L_6 Tetrahedron with Coordination Assembly Function, *J. Am. Chem. Soc.*, 2017, **139**, 16845–16851.

26 G.-H. Chen, Y.-P. He, Y. Yu, H. Lv, S. Li, F. Wang, Z.-G. Gu and J. Zhang, Post-Assembly Modification of Homochiral Titanium–Organic Cages for Recognition and Separation of Molecular Isomers, *Angew. Chem., Int. Ed.*, 2023, **135**, e202300726.

27 M.-Y. Gao, F. Wang, Z.-G. Gu, D.-X. Zhang, L. Zhang and J. Zhang, Fullerene-like Polyoxotitanium Cage with High Solution Stability, *J. Am. Chem. Soc.*, 2016, **138**, 2556–2559.

28 W.-H. Fang, L. Zhang and J. Zhang, A 3.6 nm Ti_{52}–Oxo Nanocluster with Precise Atomic Structure, *J. Am. Chem. Soc.*, 2016, **138**, 7480–7483.

29 L. Zhang, X. Fan, X. Yi, X. Lin and J. Zhang, Coordination-Delayed-Hydrolysis Method for the Synthesis and Structural Modulation of Titanium-Oxo Clusters, *Acc. Chem. Res.*, 2022, **55**, 3150–3161.

30 C. Wang, S.-J. Wang and F.-G. Kong, Calixarene-Protected Titanium-Oxo Clusters and Their Photocurrent Responses and Photocatalytic Performances, *Inorg. Chem.*, 2021, **60**, 5034–5041.

31 Y.-Q. Tian, Y.-S. Cui, W.-D. Yu, C.-Q. Xu, X.-Y. Yi, J. Yan, J. Li, C. Liu and Y.-Q. Tian, An ultrastable Ti-based metallocalixarene nanocage cluster with photocatalytic amine oxidation activity, *Chem. Commun.*, 2022, **58**, 6028–6031.

32 L.-F. Dai, X.-R. Liu, Y.-Q. Tian, X.-Y. Yi and C. Liu, Auxiliary Carboxylate-Induced Assembly of Calix[6]arene-Polyoxotitanate Hybrid Systems with Photocatalytic Activity in the Oxidation of Sulfides, *Inorg. Chem.*, 2023, **62**, 6047–6054.

33 Y.-H. Guo, Y.-Z. Yu, Y.-H. Shen, L.-G. Yang, N.-N. Liu, Z.-Y. Zhou and Y.-S. Niu, "Three-in-One" Structural-Building-Mode-Based Ti_{16}-Type Titanium Oxo Cluster Entirely Protected by the Ligands Benzoate and Salicylhydroxamate, *Inorg. Chem.*, 2022, **61**, 8685–8693.

34 M. Y. Gao, L. Zhang and J. Zhang, Acid-Controlled Synthesis of Carboxylate-Stabilized Ti_{44}-Oxo Clusters: Scaling up Preparation, Exchangeable Protecting Ligands, and Photophysical Properties, *Chem.–Eur. J.*, 2019, **25**, 10450–10455.

35 Q.-Y. Zhu and J. Dai, Titanium oxo/alkoxyl clusters anchored with photoactive ligands, *Coord. Chem. Rev.*, 2021, **430**, 213664.

36 W.-H. Fang, L. Zhang, J. Zhang and W.-H. Fang, Synthetic strategies, diverse structures and tuneable properties of polyoxo-titanium clusters, *Chem. Soc. Rev.*, 2018, **47**, 404–421.

37 J.-X. Liu, M.-Y. Gao, W.-H. Fang, L. Zhang and J. Zhang, Bandgap Engineering of Titanium–Oxo Clusters: Labile Surface Sites Used for Ligand Substitution and Metal Incorporation, *Angew. Chem., Int. Ed.*, 2016, **55**, 5160–5165.

38 W.-D. Liu, G.-J. Li, H. Xu, Y.-K. Deng, M.-H. Du, L.-S. Long, L.-S. Zheng, X.-J. Kong and W.-D. Liu, Circularly polarized luminescence and performance modulation of chiral europium-titanium (Eu_2Ti_4)-oxo clusters, *Chem. Commun.*, 2023, **59**, 346–349.

39 H. Zheng, M.-H. Du, S.-C. Lin, Z.-C. Tang, X.-J. Kong, L.-S. Long and L.-S. Zheng, Assembly of a Wheel-Like $Eu_{24}Ti_8$ Cluster under the Guidance of High-Resolution Electrospray Ionization Mass Spectrometry, *Angew. Chem., Int. Ed.*, 2018, **57**, 10976–10979.

40 X. Fan, F. Yuan, D. Li, S. Chen, Z. Cheng, Z. Zhang, S. Xiang, S.-Q. Zang, J. Zhang and L. Zhang, Threefold Collaborative Stabilization of Ag_{14}-Nanorods by Hydrophobic Ti_{16}-Oxo Clusters and Alkynes: Designable Assembly and Solid-State Optical-Limiting Application, *Angew. Chem., Int. Ed.*, 2021, **133**, 13059–13064.

41 Y.-Z. Yu, Y.-R. Zhang, C.-H. Geng, L. Sun, Y. Guo, Y.-R. Feng, Y.-X. Wang and X.-M. Zhang, Precise and Wide-Ranged Band-Gap Tuning of Ti_6-Core-Based Titanium Oxo Clusters by the Type and Number of Chromophore Ligands, *Inorg. Chem.*, 2019, **58**, 16785–16791.

42 C. Liu, J. Hu, W. Liu, F. Zhu, G. Wang, C. H. Tung and Y. Wang, Binding Modes of Salicylic Acids to Titanium Oxide Molecular Surfaces, *Chem.–Eur. J.*, 2020, **26**, 2666–2674.

43 J. B. Benedict and P. Coppens, The Crystalline Nanocluster Phase as a Medium for Structural and Spectroscopic Studies of Light Absorption of Photosensitizer Dyes on Semiconductor Surfaces, *J. Am. Chem. Soc.*, 2010, **132**, 2938–2944.

44 K. Gigant, A. Rammal and M. Henry, Synthesis and Molecular Structures of Some New Titanium(IV) Aryloxides, *J. Am. Chem. Soc.*, 2001, **123**, 11632–11637.

45 J.-L. Hou, P. Huo, Z.-Z. Tang, L.-N. Cui, Q.-Y. Zhu and J. Dai, A Titanium Oxo Cluster Model Study of Synergistic Effect of Co-coordinated Dye Ligands on Photocurrent Responses, *Inorg. Chem.*, 2018, **57**, 7420–7427.

46 C. Liu, J. Hu, F. Zhu, J. Zhan, L. Du, C. H. Tung and Y. Wang, Functionalization of Titanium Oxide Cluster $Ti_{17}O_{24}(OC_3H_7)_{20}$ with Catechols: Structures and Ligand-Exchange Reactivities, *Chem.–Eur. J.*, 2019, **25**, 14843–14849.

47 M.-Y. Gao, Z. Wang, Q.-H. Li, D. Li, Y. Sun, Y. H. Andaloussi, C. Ma, C. Deng, J. Zhang and L. Zhang, Black Titanium-Oxo Clusters with Ultralow Band Gaps and Enhanced Nonlinear

Optical Performance, *J. Am. Chem. Soc.*, 2022, **144**, 8153–8161.

48 G. Fornasieri, L. Rozes, S. Le Calvé, B. Alonso, D. Massiot, M. N. Rager, M. Evain, K. Boubekeur and C. Sanchez, Reactivity of Titanium Oxo Ethoxo Cluster $[Ti_{16}O_{16}(OEt)_{32}]$. Versatile Precursor of Nanobuilding Block-Based Hybrid Materials, *J. Am. Chem. Soc.*, 2005, **127**, 4869–4878.

49 H.-L. Zhai, J.-L. Hou, C.-Y. Luo, L.-J. Ma, Q.-Y. Zhu and J. Dai, Photocurrent and Gelation Properties of Polyphenol-Modified Titanium-Oxo Compounds, *Inorg. Chem.*, 2022, **61**, 13191–13198.

50 A. J. Surman, P. J. Robbins, J. Ujma, Q. Zheng, P. E. Barran and L. Cronin, Sizing and Discovery of Nanosized Polyoxometalate Clusters by Mass Spectrometry, *J. Am. Chem. Soc.*, 2016, **138**, 3824–3830.

51 Z. Wang, R. K. Gupta, F. Alkan, B.-L. Han, L. Feng, X.-Q. Huang, Z.-Y. Gao, C.-H. Tung and D. Sun, Dicarboxylic Acids Induced Tandem Transformation of Silver Nanocluster, *J. Am. Chem. Soc.*, 2023, **145**, 19523–19532.

52 Z. Wang, Y.-J. Zhu, B.-L. Han, Y.-Z. Li, C.-H. Tung and D. Sun, A route to metalloligands consolidated silver nanoclusters by grafting thiacalix[4]arene onto polyoxovanadates, *Nat. Commun.*, 2023, **14**, 5295.

53 Q. Yao, V. Fung, C. Sun, S. Huang, T. Chen, D.-e. Jiang, J. Y. Lee and J. Xie, Revealing isoelectronic size conversion dynamics of metal nanoclusters by a noncrystallization approach, *Nat. Commun.*, 2018, **9**, 1979.

54 Y.-J. Liu, Y.-F. Sun, S.-H. Shen, S.-T. Wang, Z.-H. Liu, W.-H. Fang, D. S. Wright and J. Zhang, Water-stable porous Al_{24} Archimedean solids for removal of trace iodine, *Nat. Commun.*, 2022, **13**, 6632.

55 H.-M. Yu, M.-H. Du, J. Shu, Y.-H. Deng, Z.-M. Xu, Z.-W. Huang, Z. Zhang, B. Chen, P. Braunstein and J.-P. Lang, Self-Assembly of Cluster-Mediated 3D Catenanes with Size-Specific Recognition Behavior, *J. Am. Chem. Soc.*, 2023, **145**, 25103–25108.

56 Q. Tang, G. Hu, V. Fung and D.-e. Jiang, Insights into Interfaces, Stability, Electronic Properties, and Catalytic Activities of Atomically Precise Metal Nanoclusters from First Principles, *Acc. Chem. Res.*, 2018, **51**, 2793–2802.

57 J. D. Sokolow, E. Trzop, Y. Chen, J. Tang, L. J. Allen, R. H. Crabtree, J. B. Benedict and P. Coppens, Binding Modes of Carboxylate- and Acetylacetonate-Linked Chromophores to Homodisperse Polyoxotitanate Nanoclusters, *J. Am. Chem. Soc.*, 2012, **134**, 11695–11700.

58 C. Wang, S. Wang, F. Kong, N. Chen and C. Wang, Ferrocene-sensitized titanium-oxo clusters with effective visible light absorption and excellent photoelectrochemical activity, *Inorg. Chem. Front.*, 2022, **9**, 959–967.

59 N. K. Chaki, S. Mandal, A. C. Reber, M. Qian, H. M. Saavedra, P. S. Weiss, S. N. Khanna and A. Sen, Controlling Band Gap Energies in Cluster-Assembled Ionic Solids through Internal Electric Fields, *ACS Nano*, 2010, **4**, 5813–5818.

60 X. Huang, S. Liu, Z. Zhou, H. Zhang, Z. Gao, G. Shen, H. Wang, Z. Wang, Q. Yao, D. Sun and X. Huang, The tail of imidazole regulated the assembly of two robust sandwich-type polyoxotungstate-based open frameworks with efficient visible-white-light-driven catalytic oxidation of sulfides, *Inorg. Chem. Front.*, 2023, **10**, 1465–1474.

61 Q. Lu and X. Wang, Recent Progress of Sub-Nanometric Materials in Photothermal Energy Conversion, *Adv. Sci.*, 2022, **9**, 2104225.

62 X. Cui, Q. Ruan, X. Zhuo, X. Xia, J. Hu, R. Fu, Y. Li, J. Wang and H. Xu, Photothermal Nanomaterials: A Powerful Light-to-Heat Converter, *Chem. Rev.*, 2023, **123**, 6891–6952.

63 Z. Wang, F. Alkan, C. M. Aikens, M. Kurmoo, Z.-Y. Zhang, K.-P. Song, C.-H. Tung and D. Sun, An Ultrastable 155-Nuclei Silver Nanocluster Protected by Thiacalix[4]arene and Cyclohexanethiol for Photothermal Conversion, *Angew. Chem., Int. Ed.*, 2022, **61**, e202206742.

64 K. Sheng, Z. Wang, L. Li, Z.-Y. Gao, C.-H. Tung and D. Sun, Solvent-Mediated Separation and Reversible Transformation of 1D Supramolecular Polymorphs Built from $[W_{10}O_{32}]^{4-}$ Templated 48-Nuclei Silver(I) Cluster, *J. Am. Chem. Soc.*, 2023, **145**, 10595–10603.

65 Z. Wang, Y.-J. Zhu, B.-L. Han, Y.-Z. Li, C.-H. Tung and D. Sun, A route to metalloligands consolidated silver nanoclusters by grafting thiacalix[4]arene onto polyoxovanadates, *Nat. Commun.*, 2023, **14**, 5295.